Metastability in an open quantum Ising model

Dominic C. Rose,[1,2,*] Katarzyna Macieszczak,[1,2,3] Igor Lesanovsky,[1,2] and Juan P. Garrahan[1,2]
[1]*School of Physics and Astronomy, University of Nottingham, Nottingham NG7 2RD, United Kingdom*
[2]*Centre for the Mathematics and Theoretical Physics of Quantum Non-Equilibrium Systems, University of Nottingham, Nottingham NG7 2RD, United Kingdom*
[3]*School of Mathematical Sciences, University of Nottingham, Nottingham NG7 2RD, United Kingdom*
(Received 22 August 2016; published 18 November 2016)

We apply a recently developed theory for metastability in open quantum systems to a one-dimensional dissipative quantum Ising model. Earlier results suggest this model features either a nonequilibrium phase transition or a smooth but sharp crossover, where the stationary state changes from paramagnetic to ferromagnetic, accompanied by strongly intermittent emission dynamics characteristic of first-order coexistence between dynamical phases. We show that for a range of parameters close to this transition or crossover point the dynamics of the finite system displays pronounced metastability, i.e., the system relaxes first to long-lived metastable states before eventual relaxation to the true stationary state. From the spectral properties of the quantum master operator we characterize the low-dimensional manifold of metastable states, which are shown to be probability mixtures of two, paramagnetic and ferromagnetic, metastable phases. We also show that for long times the dynamics can be approximated by a classical stochastic dynamics between the metastable phases that is directly related to the intermittent dynamics observed in quantum trajectories and thus the dynamical phases.

DOI: 10.1103/PhysRevE.94.052132

I. INTRODUCTION

Through the use of experimental platforms such as ultracold atomic gases, trapped ions, and Rydberg atoms a wide range of nonequilibrium phenomena in open quantum many-body systems have now been realized [1–6]. This has been accompanied by a significant increase in the theoretical understanding of such systems numerically, through the use of techniques adapted from atomic-optics and closed quantum systems [7], and analytically via field-theoretical methods [8,9], among other approaches.

One question of interest addressed by theoretical studies of nonequilibrium open many-body quantum systems has been the understanding of the phase structure of the stationary state, given the possibility that these systems display phase transitions—singular changes in the stationary state in the limit of large system size—which may be distinct from those of equilibrium systems. The aim of many of such studies has been to characterize the phase structure of nonequilibrium steady states via static order parameters, such as the magnetization in spin systems, and spatial correlation functions more generally, see, e.g., Refs. [8–10]. However, even in the case where such transitions are not present, the dynamics of these systems can be very rich and cooperative. One way to uncover this dynamical complexity via large-deviation methods (such as the "thermodynamics of trajectories," see, e.g., Refs. [11,12], or the related full-counting statistics, see, e.g., Refs. [13]), which allow us to define and characterize dynamical phases where order parameters are dynamic time-integrated observables, such as total count of emissions into the environment.

In this paper we focus on a different aspect of open quantum many-body systems, that of *metastability* of the dynamics. Metastability is a characteristic feature of the dynamics of slow relaxing systems, namely, the partial relaxation into long-lived states before eventual decay to the true stationary state. This is a consequence of separation of time scales in the dynamics. In such systems the transient dynamics will appear nonergodic, in the sense that different initial conditions will relax to different metastable states, before ergodicity is eventually restored. In classical systems, metastable behavior typically occurs in two distinct situations: one is in the dynamics near a (usually first-order) static phase transition [14], where metastable dynamics is intimately related to the existence of static phases; the second one is in glass forming systems [15] where metastable behavior is not obviously related to any static features (see, e.g., Ref. [16] for various viewpoints on this issue).

Here we focus on the first instance above for the case of a many-body quantum system subject to dissipation where metastability can be traced back to distinct features of its stationary properties, a transverse field Ising model with on-site dissipative decay [9,17–24]. We study the dynamics of this model by means of a recent theory for metastability in open quantum systems [25]. This new approach is a generalization to open quantum systems, evolving according to a Lindblad master equation [26–28], of the method of Refs. [29–33] for classical Markovian systems. This approach relies on the fact that metastable behavior necessarily results from a separation of eigenmodes in the spectrum of the master operator generating the dynamics, thus allowing one to investigate both the structure of the metastable states and the long-time dynamics of the system using a reduced number of parameters [25,34]. The metastable states form a metastable manifold (MM), a convex subset of the system states (see Fig. 1, details in Sec. II) on which the long-time dynamics takes place [25]. In Ref. [25] this approach was applied to few-body models more related to problems in quantum information. Here we demonstrate the effectiveness of this approach for a many-body system where metastability emerges cooperatively with increasing system size. The dissipative Ising model we consider is also of particular interest as it can be realized experimentally through the use of Rydberg atoms in optical

*dominic.rose@nottingham.ac.uk

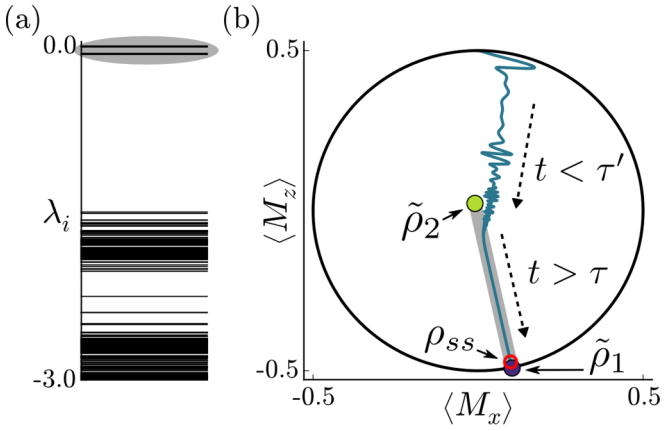

FIG. 1. (a) Real part of the spectrum of the master operator of the open quantum Ising model defined in Sec. III, for size $N = 7$, with spin interaction $V/\kappa = 250$ and transverse field $\Omega/\kappa = 50$, where κ is decay rate. Spectrum is plotted in units of κ. The two eigenvalues with largest real parts, $\lambda_{1,2}$, highlighted in gray, correspond to the only eigenmodes that contribute to the dynamics at long times. The large gap to the next eigenvalue, λ_3, causes metastability in the dynamics. (b) The metastable manifold (MM) induced by the spectral structure of (a). System states are represented by the average total magnetization per spin in the x and z directions. The MM (gray line) is bounded by two extreme metastable states $\tilde{\rho}_1$ (purple dot) and $\tilde{\rho}_2$ (green dot). The evolution from an initial state $\rho_\uparrow$ of all spins up (blue curve) undergoes a fast evolution for $t \ll \tau' = -1/\lambda_3$ onto the MM. After a long period of apparent stationarity ($\tau' \ll t \ll \tau = -1/\lambda_2$), the states on the MM evolve towards the true stationary state ρ_{ss} (red circle) for $t \gg \tau$.

lattices [17,19]. It may also be possible to realize it using circuit quantum electrodynamics (QED) [18] as these systems are intrinsically open; however, it may be difficult to control the exact nature of the interaction with the environment.

The dissipative quantum Ising model we study here has the basic ingredients of a system where metastability is a dynamical consequence of static features. In order to clarify what we mean, consider, for example, a classical ferromagnet at low temperatures in the thermodynamic limit [14]. For such a system, if one starts close to the coexistence point (say, at small positive magnetic field) but in a state belonging to the wrong phase (in this case with initial negative magnetization), there will be an initial fast relaxation within this phase, before a much longer relaxation to the eventual equilibrium state within the stable phase (of positive magnetization). This occurs due to the existence of a large, but finite, free-energy barrier that needs to be crossed from the metastable phase to the stable phase. Hysteretic behavior is a manifestation of this phenomenon. Furthermore, zero field is the point of a first-order transition, and there is strict coexistence between the phases of positive and negative magnetization, which means that each is stable at long times, giving rise to ergodicity breaking. It is important to note that such a transition only occurs in the thermodynamic limit. For finite size, even at zero field, dynamics is metastable, with the metastable states being those of nonzero magnetization, and the true stationary state that of paramagnetic equilibrium. Dynamics in this case will also be intermittent, displaying many "magnetization reversals" [14]. In this sense, metastability which has its origin in distinct static "phases" does not require the presence of a strict phase transition, only that the "phases" are long lived and kinetically only weakly connected (in the example of the ferromagnet, separated by a free-energy barrier that is large compared to temperature). In fact, usually the simplest way to anticipated such a structure is from a mean-field approximation, even if there is no singular transition in the exact problem.

Previous work [19] on the dissipative quantum Ising model suggested a bistable character to the stationary state of this system. Within a mean-field approximation [19], this model has a region of its parameter space in which it exhibits a strict first-order coexistence, terminating at a critical point, between ferromagnetic and paramagnetic steady states. Related to this, dynamics of this model in one dimension for finite size was shown to display pronounced intermittency between periods of photon emission activity and inactivity in quantum jump trajectories [19]. While the mean-field approximation is not necessarily expected to be accurate even in the thermodynamic limit in one dimension [9,20,21], it does provide an idea of the basic phase structure of the model. As in the case discussed above of a classical ferromagnet, for metastability to be present all that is required is that states with distinct static character are approximate stationary states of the dynamics. Using the methods of Ref. [25] we show the relation between the ferromagnetic or paramagnetic states that mean-field suggest and the metastable states of the dynamics of the dissipative quantum Ising model at finite size. We show that the short-time dynamics relaxes to the metastable manifold in a way that is dependent on initial states (i.e., apparent but transient nonergodicity). We further show that the long-time evolution within the MM is that of an effective classical stochastic dynamics, even though the underlying many-body system features quantum effects. This is in line with recent field-theoretic studies of open spin lattices, which show the long-time properties of similar models are often classical [8,9].

The paper is organized as follows. In Sec. II we briefly review the spectral approach to metastability in open quantum systems, along with the effective long-time description, giving a particular focus to the case when the MM is one dimensional (1D) as is the case for the dissipative quantum Ising model. Section III provides an in-depth analysis of metastability in the model. We begin in Sec. III A by returning to the mean-field approach used in Ref. [19], but focusing on time evolution instead of only steady state(s) and discussing the effect of neglecting fluctuations from spatial correlations. We then apply the spectral approach of Ref. [25] to the exact model of $N = 7$ spins and find a parameter regime where the system is metastable (Sec. III B). This is followed by characterization of the MM in terms of the properties of metastable phases (Sec. III C). In Sec. III D we show how metastability can be observed in the behavior of expectation values and autocorrelations of system observables. Finally, we demonstrate how the metastability in the spin magnetization and the effective dynamics within the MM manifests in individual realizations of the system evolution through intermittency in activity of quantum trajectories (Sec. III E).

II. METASTABLE MANIFOLDS AND EFFECTIVE EVOLUTION

In this section we review the theory for metastability in open quantum systems with Markovian dynamics introduced recently in Ref. [25]. Evolution of a system state described by the density matrix ρ is generated by the Lindblad master operator

$$\mathcal{L}(\rho) = -i[H,\rho] + \sum_j \left[J_j \rho J_j^\dagger - \frac{1}{2}\{J_j^\dagger J_j, \rho\}\right], \quad (1)$$

i.e., $d\rho/dt = \mathcal{L}(\rho)$ [27,28]. Here H is the Hamiltonian of the system and the jump operators J_j mediate the system-bath interaction, providing coupling of the system to the surrounding environment. If these interactions lead to emissions of a quanta of energy, e.g., photons being emitted by atoms coupled to the vacuum electromagnetic field, then the action of jump operators can be detected through continuous measurements, e.g., photon counting [19].

Since this operator acts linearly on the density matrix, the evolution it generates can be understood in terms of its eigenvalues and eigenmatrices [35]. Let the eigenvalues of the master operator be $\lambda_k = \lambda_k^R + i\,\lambda_k^I$, with λ_k^R and λ_k^I representing the real and imaginary parts, respectively. These are ordered such that $|\lambda_k^R| \leqslant |\lambda_{k+1}^R|$. Note that the real parts are necessarily less than or equal to 0, with 0 corresponding to steady states, due to the (completely) positive trace-preserving evolution generated by the master operator, Eq. (1). Further note that, due to the hermiticity preservation of the master operator, eigenvalues must come in conjugate pairs and in particular that if the real part is nondegenerate the eigenvalue must hence be purely real. Let the left and right eigenmatrices (note that $\mathcal{L}$ is not Hermitian in general) associated to λ_k be denoted L_k and R_k, respectively. We choose normalization such that $\mathrm{Tr}(L_k R_{k'}) = \delta_{kk'}$. Generically, the steady state ρ_{ss} is unique (as is the case for the finite-size dissipative Ising chain discussed in this work) and we further normalize it such that $\mathrm{Tr}(\rho_{\mathrm{ss}}) = 1$ and thus also $L_1 = \mathbb{1}$. Defining $c_k = \mathrm{Tr}[\rho(0)L_k]$, for an initial system state $\rho(0)$, the system state at time t is given by

$$\rho(t) = e^{t\mathcal{L}}[\rho(0)] = \rho_{\mathrm{ss}} + \sum_k c_k e^{t\lambda_k} R_k. \quad (2)$$

We are interested in metastable behavior. Therefore we assume there is a large separation in the values of the real parts of the eigenvalues, $|\lambda_m^R| \ll |\lambda_{m+1}^R|$, cf. Fig. 1(a), and denote the corresponding time scales by $\tau = -1/\lambda_m^R$ and $\tau' = -1/\lambda_{m+1}^R$. If we consider times $t \gg \tau'$, then we may neglect terms beyond the mth in the sum in Eq. (2). For $t \ll \tau$, we also have $e^{t\lambda_k} \approx 1$ for $k \leqslant m$, and the reduced expansion defines metastable states of the system, see Fig. 1. Thus, the projection $\mathcal{P}$ onto the MM is given by $\mathcal{P}\rho = \mathrm{Tr}(\rho)\rho_{\mathrm{ss}} + \sum_{k=2}^m c_k R_k$. Furthermore, note that the MM is determined by a subset in $\mathbb{R}^{m-1}$ given by the coefficients $\{c_k\}_{k=1}^m$, whose values are bounded by the maximum and minimum eigenvalues of the relevant left eigenmatrices. For times $t \gg \tau'$, only the first m modes contribute to the system dynamics, cf. Eq. (2). Therefore dynamics takes place essentially only inside the MM and is effectively generated by the projection of the master operator on the MM, $\mathcal{L}_{\mathrm{eff}} = \mathcal{P}\mathcal{L}\mathcal{P}$.

A. Metastable manifold

The general structure for MMs is discussed in Ref. [25]. We will see in Sec. III B that for the open quantum Ising model the MM is one dimensional, that is, $m = 2$, which is the case we now restrict ourselves to. The basis for the MM is given by ρ_{ss} and R_2, but R_2 lacks interpretation as a state of the system since $\mathrm{Tr}(R_2) = 0$ due to trace-preserving dynamics. Instead, we can make use of the convexity of the MM (inherited from the convexity of the full space of density matrices) to consider metastable states as a linear combination of the states at either end of the MM, which we call *extreme metastable states* (eMSs) [25],

$$\tilde{\rho}_1 = \rho_{\mathrm{ss}} + c_2^{\max} R_2, \quad (3)$$

$$\tilde{\rho}_2 = \rho_{\mathrm{ss}} + c_2^{\min} R_2, \quad (4)$$

where $c_2^{\max}$ and $c_2^{\min}$ are the maximum and minimum eigenvalues of the Hermitian L_2, respectively.

Writing $\mathcal{P}\rho = p_1\tilde{\rho}_1 + p_2\tilde{\rho}_2$ and using $p_1 = 1 - p_2$ (from convexity of the MM), the coeffcients $p_{1,2}$ are given by the expectation value, $p_{1,2} = \mathrm{Tr}(\tilde{P}_{1,2}\rho)$, of the observables

$$\tilde{P}_1 = \left(L_2 - c_2^{\min} I\right)/\Delta c_2, \quad (5)$$

$$\tilde{P}_2 = \left(-L_2 + c_2^{\max} I\right)/\Delta c_2, \quad (6)$$

where $\Delta c_2 = c_2^{\max} - c_2^{\min}$.

As $\tilde{\rho}_1$, $\tilde{\rho}_2$ are the eMSs, the coeffcients are necessarily positive, $p_{1,2} \geqslant 0$, leading to the interpretation of any state on the MM as a probabilistic mixture of the two eMSs. Thus, $\tilde{\rho}_1$ and $\tilde{\rho}_2$ constitute two metastable phases and one can understand the properties of all metastable states by characterizing the properties of only these two, as done in Sec. III C. For a basis of any other two states on the MM, one of the coefficients would necessarily be negative for certain parts of the MM.

B. Effective dynamics within metastable manifold

The evolution for times $t \gg \tau$ effectively takes place on the metastable manifold towards the steady state [25]. Noting that λ_2 must be real and thus dropping the R superscript, the generator $\mathcal{L}_{\mathrm{eff}} = \mathcal{P}\mathcal{L}\mathcal{P}$ can be now expressed in the basis of the eMSs, cf. Eqs. (3)–(6), as

$$\mathcal{L}_{\mathrm{eff}} = \frac{-\lambda_2}{\Delta c_2}\begin{pmatrix} -c_2^{\max} & -c_2^{\min} \\ c_2^{\max} & c_2^{\min} \end{pmatrix}, \quad (7)$$

yielding the dynamics of the probabilites p_1, p_2 as $d\mathbf{p}/dt = \mathcal{L}_{\mathrm{eff}}\,\mathbf{p}$, where $\mathbf{p}^T = (p_1, p_2)$. Note that the entries in each column of $\mathcal{L}_{\mathrm{eff}}$ add to 0, which corresponds to probability conservation. Moreover, since $\lambda_2 < 0$ and $c_2^{\max} > 0$, $c_2^{\min} \leqslant 0$ [as $\mathrm{Tr}(L_2\rho_{\mathrm{ss}}) = 0$ by orthogonality of eigenmodes], the diagonal elements are negative and the off-diagonal positive, which ensures positivity of the dynamics. Thus, $\mathcal{L}_{\mathrm{eff}}$ is a generator of classical stochastic dynamics between two metastable phases, $\tilde{\rho}_1$ and $\tilde{\rho}_2$.

Note that the dynamics induced by $\mathcal{L}_{\mathrm{eff}}$ between $\tilde{\rho}_1$ and $\tilde{\rho}_2$ satisfies the detailed balance, with the exit time from a metastable phase given by the inverse of the diagonal entry, e.g., $(-c_2^{\max}\lambda_2)^{-1} = \tau\,(c_2^{\max})^{-1}$ for $\tilde{\rho}_1$, and the stationary

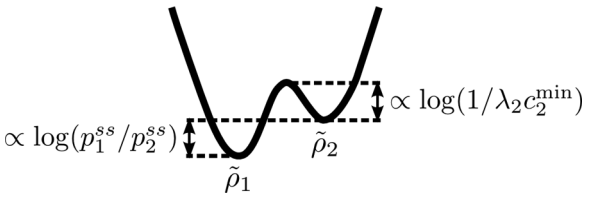

FIG. 2. Illustration of the two-basin analogy of metastability when the metastable manifold is one dimensional. The figure represents a one-dimensional Landau free energy. The two eMSs are analogous to the two free-energy basins corresponding to two phases of the system, and their free-energy difference is analgous to the logarithm of their relative probabilities. In the thermodynamic case, the time scale for connecting the basins is the exponential of the free-energy barrier (divided by temperature—the usual Arrhenius law for thermal escape). In this sense, since in our dynamical case the time scale is controlled by the gap, the log of the gap is analogous to the barrier. See the main text for discussion.

probability determined by the ratio of the off-diagonal terms, $-c_2^{\min}/c_2^{\max}$, independent from τ.

This dynamics is analogous to the effective long-time dynamics in finite classical systems close to conditions where coexistence between two stable phases appears in the thermodynamic limit, such as, for example, a two-dimensional classical Ising model at low temperature in the ferromagnetic phase with small negative magnetic field favoring magnetization down [14,36]. Intuitively, one can imagine such a situation in terms of motion in a Landau free energy, a function of a collective variable such as magnetization, which features two minima corresponding to the two competing phases, one of positive magnetization and a favored one of negative magnetization, cf. Fig. 2. The height of the barrier between the two wells is related to the surface tension of creating droplets of one phase in a background of the other. In finite systems (or away from the coexistence point in the thermodynamic limit) this barrier can be overcome by thermal fluctuations. When temperature is low, such that thermal fluctuations are weak, an initial configuration of all spins down would initially relax via small-scale fluctuations within the positive magnetization phase (intuitively "rolling down the hill" towards its closest free-energy minimum) for $t \gg \tau'$. At longer times, $t \sim \tau$ (dependent on the height of the barrier separating the wells, typically in an Arrhenius fashion for the case of thermal excitations), large-enough domains of the spin-down phase are created, allowing the system to overcome the free-energy barrier. The subsequent switching dynamics between the two basins leads at long times to equilibration. Note that, due to detailed balance, the ratio of the occupation in the equilibrium state between the two wells depends on the difference of the free energies, not the barrier height, which only sets the relaxation time.

C. Observation of metastability

Metastability of the system dynamics can be observed in the behavior of expectation values and autocorrelations of system observables [25,37]. In Sec. III D we focus on measuring a given spin magnetization (or, equivalently, the probability distribution of the magnetization). For long times $t \gg \tau'$ the exact dynamics should be captured by the effective long-time description, see Eq. (7), and for the expectation value of an observable O we arrive at

$$\langle O(t)\rangle \approx \mathbf{o}^T\, \mathbf{p}(t), \tag{8}$$

where $\mathbf{o}_i = \mathrm{Tr}(O\tilde{\rho}_i)$. Observation of the metastability in the expectation value requires preparation of an initial system state that differs from the steady state. Nevertheless, for the system in the steady state, metastability can be observed in the time autocorrelation of measurements of a system observable. When time between measurements is greater than τ', the state conditioned on the initial measurement relaxes into the MM and

$$C(t) = \langle O(t)O(0)\rangle = \mathrm{Tr}(Oe^{t\mathcal{L}}\mathcal{O}\rho_{\mathrm{ss}}) \approx \mathrm{Tr}(Oe^{t\mathcal{L}_{\mathrm{eff}}}\mathcal{P}\mathcal{O}\rho_{\mathrm{ss}}), \tag{9}$$

where $\mathcal{O}$ is the superoperator representing measurement of the observable O. As $\mathcal{P}\rho_{\mathrm{ss}} = \rho_{\mathrm{ss}}$, we have

$$C(t) \approx \mathbf{o}^T\, e^{t\mathcal{L}_{\mathrm{eff}}}\, \mathbf{O}\, \mathbf{p}_{\mathrm{ss}}, \tag{10}$$

where $\mathbf{O}_{ij} = (\mathcal{P}\mathcal{O}\mathcal{P})_{ij} = \mathrm{Tr}[\tilde{P}_i\mathcal{O}(\tilde{\rho}_j)]$ and $\mathbf{p}_{\mathrm{ss}}^T = (-c_2^{\min}/\Delta c_2, c_2^{\max}/\Delta c_2)$ is the stationary probability of ρ_{ss} between the metastable phases.

III. OPEN QUANTUM ISING MODEL

We now apply the theory [25] reviewed in the previous section to a dissipative quantum many-body system, an open version of the 1D transverse field Ising model, consisting of a chain of N spin-1/2 particles with periodic boundary conditions coupled to an external bath. The Hamiltonian is given by

$$H = \Omega \sum_{j=1}^{N} S_x^{(j)} + V \sum_{i=1}^{N} S_z^{(j)} S_z^{(j+1)}, \tag{11}$$

where Ω describes the transverse magnetic field and V the interaction between neighboring spins. The spin operators $S_\alpha^{(j)} = \frac{1}{2}\sigma_\alpha^{(j)}$, where $\alpha = \{x,y,z\}$. The jump operators mediating the interaction with the bath couple to individual spins,

$$J_j = \sqrt{\kappa}\, S_-^{(j)} = \sqrt{\kappa}\left(S_x^{(j)} - i\, S_y^{(j)}\right), \tag{12}$$

where the decay rate κ is determined by strength of system-bath coupling, and $j = 1,\ldots,N$. This system can be realized using Rydberg atoms [17,38], in which case the jumps can be seen to be photon emissions from individual spins into the environment. The properties of these jump operators imply that the system dynamics are irreducible and the stationary state unique for all finite N [39].

The order parameters we will consider are the magnetizations along each axis,

$$M_\alpha = \frac{1}{N}\sum_{j=1}^{N} S_\alpha^{(j)}. \tag{13}$$

We will find in Sec. III D and III E that the z component of the magnetization in particular is sufficient to highlight metastable dynamics in this system.

A. Time-dependent mean-field approximation

We start our analysis by returning to the mean-field approximation studied previously in Ref. [19], this time, however, focusing on the dynamics rather than just the steady state. From the study of classical systems it is common for such an approach to give qualitatively the short-time dynamics leading to the MM, since often long-time relaxation is nonperturbative and triggered by spatial fluctuations that are dismissed at the mean-field level, see, e.g., Ref. [15]. We therefore expect to uncover within this approximation properties of the dynamics of the exact problem in its approach to the metastable regime ($t \ll \tau$). In the next subsections we consider the whole dynamical regime by considering the full spectral properties of the exact problem.

In this subsection we proceed as follows: We consider an approximation of the density matrix in the form of an arbitrary product state, i.e., $\rho_N = {\rho_1}^{\otimes N}$, where $\rho_1 = \frac{1}{2}\mathbb{1} + xS_x + yS_y + zS_z$. Note that here $x,y,z = \langle M_x\rangle, \langle M_y\rangle, \langle M_z\rangle$. These coefficients are time dependent, and we substitute this into the master operator, proceeding to trace out all but one spin, i.e., $d\rho_1/dt = \mathrm{Tr}_{2,\ldots,N}[\mathcal{L}(\rho)]$. This process gives a set of three nonlinear differential equations on the coefficients given by

$$\begin{aligned}\dot{x} &= -\frac{\kappa}{2}x - 2Vyz,\\ \dot{y} &= -\frac{\kappa}{2}y + 2Vxz - \Omega z,\\ \dot{z} &= -\frac{\kappa}{2}(1+2z) + \Omega y.\end{aligned} \tag{14}$$

The dynamics induced by these equations is highly oscillatory, with rotations about the x axis induced by the transverse field Ω, see Fig. 3(a), and rotations about the z axis—weighted by the magnetization $\langle M_z\rangle$, thus no rotation in the $z = 0$ plane, Fig. 3(c), due to the spin-spin interaction with potential V. These oscillations are eventually damped by the decaying terms proportional to κ.

Stationary solutions. The steady states of this system of equations are found from the solution of $\dot{x} = 0$, $\dot{y} = 0$, and $\dot{z} = 0$, which gives rise to a third-order polynomial in z, see Ref. [19]. There is either one or two stable real solutions depending on the parameters chosen, with the set of parameters giving bistable dynamics lying between two "spinodal" lines, see Fig. 3(g). Outside this region, the unique stationary state is ferromagnetic ($z \approx -0.5$) for small Ω and close to paramagnetic (x,y,z small) for large Ω. Inside the bistable region one of the two stationary states corresponds to a paramagnetic state while the other transitions smoothly from ferromagnetic to paramagnetic with increasing Ω. The two steady states are shown on the flow diagrams in Figs. 3(a)–3(c).

Since the mean-field approach is expected to capture the short-time evolution, we anticipate the two steady states to be qualitatively similar in properties to the eMS of the exact model. In order to compare the mean-field approximation with the exact dynamics during the metastable regime, we investigate the average asymptotic magnetization, $\overline{m}_\infty$, reached from pure initial states ρ_1 sampled uniformly from the Bloch sphere, Fig. 3(g), i.e., the magnetization of the steady state reached according to Eq. (14) (see also Ref. [40]). Outside of the bistable regime this is simply the magnetization of the unique mean-field steady state, m_{ss}. Within the bistable regime, $\overline{m}_\infty$ is the linear combination obtained from adding up the area of the basins of attraction for the two mean-field steady states, Figs. 3(d)–3(f), multiplied by their respective magnetizations.

For low Ω the basins are fairly even in size, giving a sharp transition at the left spinoidal line from $m_{\mathrm{ss}} \approx -0.5$ of the unique ferromagnetic steady state to $\overline{m}_\infty \approx -0.25$, cf. Figs. 3(d)–3(f). As Ω increases the area of the basin for the

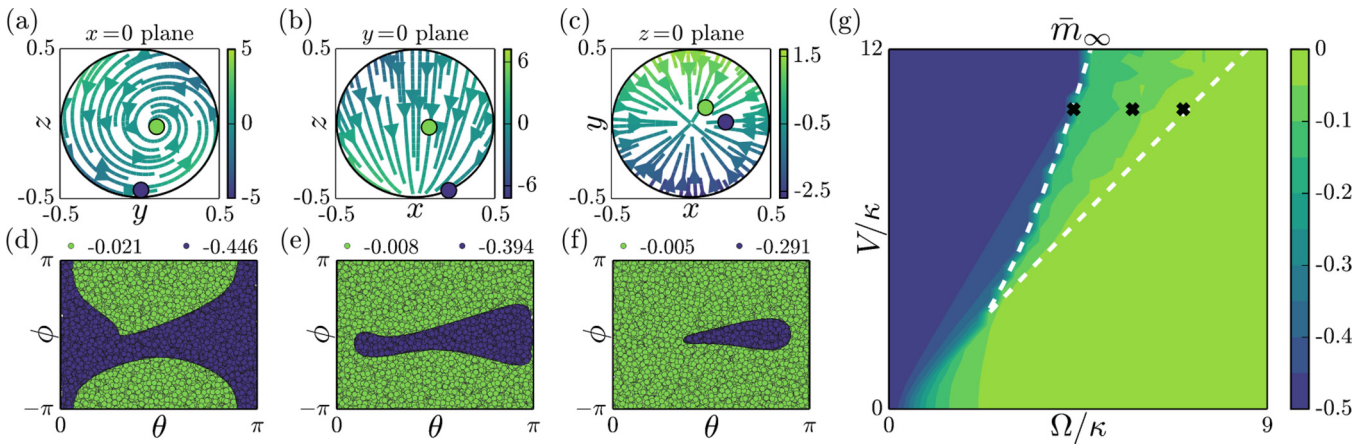

FIG. 3. [(a)–(c)] Flow induced on cross sections of the Bloch ball by the dynamics in Eq. (14) for parameters $V/\kappa = 10$, $\Omega/\kappa = 4.4$ where the system is bistable. The color of the line indicates the magnitude of the component perpendicular to the plane. The green and purple dots correspond to the two stationary solutions of the mean-field approximation projected onto the planes through the Bloch sphere. [(d)–(f)] Basins of attraction of the two mean-field stationary solutions, with the indicated values of $\langle M_z\rangle$, at three points in the bistable regime with parameters $V/\kappa = 10$ and $\Omega/\kappa = 4.4, 5.8, 7.0$, respectively, marked by black crosses in panel (g). (g) Mean-field phase diagram: $\overline{m}_\infty$, as a function of model parameters. Spinodal lines separating one-solution from two-solution regions are indicated by white dashed lines.

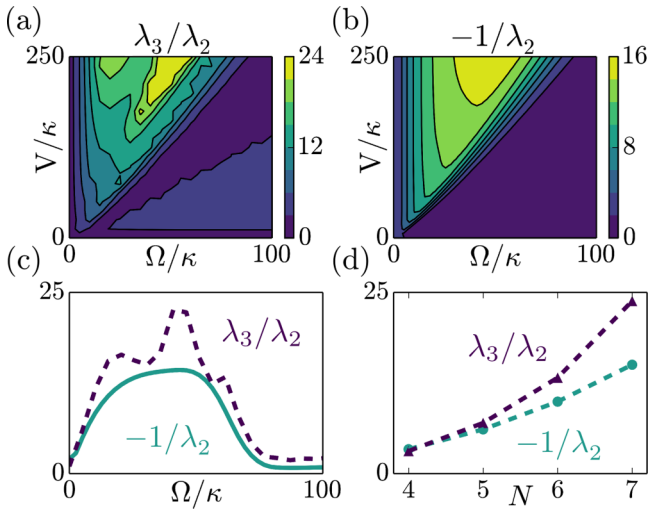

FIG. 4. (a) The ratio of the real parts of the second and third eigenvalues λ_3/λ_2, plotted over a region of the parameter space $0 \leqslant V \leqslant 250$ and $0 \leqslant \Omega \leqslant 100$. (b) The inverse gap $-1/\lambda_2$ plotted over the same region. (c) A cross section of plots (a) and (b) for $V = 200$. The dashed (purple) line is the ratio while the solid (blue) line is the inverse gap. (d) The scaling of the maximum value of the ratio (purple triangles) and inverse gap (blue circles) in this range of parameters with system size.

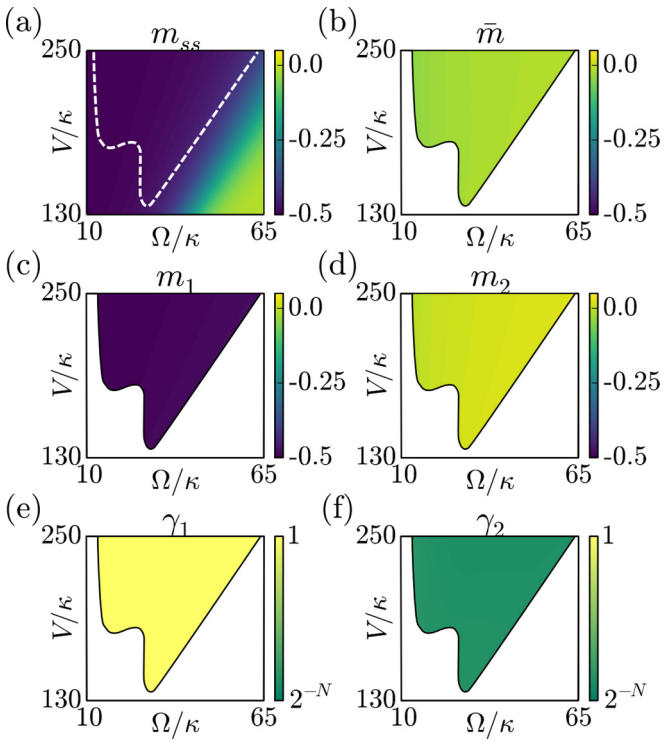

FIG. 5. (a) Magnetization of the steady state m_{ss}. The approximate boundary of the metastable region is indicated by the dashed white line. (b) The average z magnetization $\bar{m}$ in the metastable regime. In this and the following panels we only show the area where metastability holds. [(c) and (d)] Expected z magnetizations $m_i = \mathrm{Tr}(M_z\tilde{\rho}_i)$ and [(e) and (f)] purities $\gamma_i = \mathrm{Tr}(\tilde{\rho}_i^2)$ of the two metastable phases.

steady state with a lower magnetization shrinks continuously, along with the magnetization of this state increasing, with the area of the basin vanishing at the right spinoidal line, leading to a smooth increase of $\overline{m}_\infty$ to $m_{ss} \approx 0$. Below we consider the exact dynamics of a finite chain. We will see that the magnetization, averaged over a uniform distribution of initial states, behaves during the metastable regime in a similar way to the mean-field result above.

B. Spectral analysis of the master operator

Next we explore how the features of the mean-field treatment manifest in the exact master equation dynamics. For this consider numerically a system with $N = 7$ spins. We make use of the system translation invariance to first block diagonalize the master operator [41,42]. Note we find both λ_2 and λ_3 to be real and thus drop the R superscript.

For metastability we require separation in the real part of the spectrum of the Lindbladian, and we find that for this system this occurs between the second and third eigenvalues, so $m = 2$ and the metastable manifold is 1D, see Figs. 1(a) and 4(b). The parameter region of metastable dynamics– - light yellow wedge in Fig. 4(a)—is suggestive of identification with the bistable region of the mean-field approximation, cf. Fig. 3(g), with a stretching to lower values of the transverse field. The separation in the spectrum is mainly due to the the spectral gap, $-\lambda_2$, getting small, Figs. 4(b) and 4(c). Metastability in the dissipative Ising model is a collective phenomenon, since the ratio λ_3/λ_2 increases with size, as does the inverse of the gap $-1/\lambda_2$, see Fig. 4(d).

It remains an open question whether the gap strictly closes for some combination of parameters in the thermodynamic limit, as in the mean-field approximation. This would correspond to a phase transition in the stationary state of the system. What the mean-field approximation predicts is that this would be a transition between phases of different magnetization, cf. the states at either side of the bistable region, Fig. 3(g). Irrespective of whether there is a true transition in the thermodynamic limit, or a smooth but sharp crossover, the decrease of the gap with increasing size, Fig. 4(d), indicates that metastability is a consequence of the proximity to this transition or crossover point. The system sizes accessible to numerics are far from large, therefore precluding a singular transition. Dependence on size, however, indicates that such a change (whether a transition or sharp crossover) in the steady state magnetization, $m_{ss} = \mathrm{Tr}(M_z\rho_{ss})$, from the ferromagnetic state at small Ω, $m_{ss} \approx -1/2$, to the paramagnetic one at large Ω, $m_{ss} \approx \mathrm{Tr}(M_x\rho_{ss}) \approx \mathrm{Tr}(M_y\rho_{ss}) \approx 0$, should become very pronounced at large sizes. See Fig. 5(a).

C. Characterization of the metastable manifold

The metastable manifold can be characterized by the properties of two eMSs defined by Eqs. (3) and (4), which we investigate below. These two eMSs correspond to ferromagnetic ($m_1 \approx -0.5$) and paramagnetic ($m_2 \approx 0$) states, see Figs. 5(c) and 5(d). Note that the similarity between the values of m_1 and m_2 resemble the magnetizations of two stationary states in the mean-field approximation, cf. Fig. 3(d)–3(f).

We consider now the behavior of the magnetization in the z direction, $\langle M_z \rangle$, during the metastable regime taken on average by pure initial states $|\psi\rangle$, see Fig. 5(b), i.e., $\overline{m} = \overline{\mathrm{Tr}(M_z \mathcal{P}|\psi\rangle\langle\psi|)}$, where the bar denotes average with respect to uniform sampling of $|\psi\rangle$. For most of the parameter regime where metastability is present, we have $\overline{m} \approx 0$, with a transition at small Ω. This is analogous to $\overline{m}_\infty$ in the mean-field case, cf. Fig. 3(g). Here the size of the basins of attraction (given by $\frac{1}{N}\mathrm{Tr}\tilde{P}_1$ and $\frac{1}{N}\mathrm{Tr}\tilde{P}_2$, respectively) are imbalanced towards the paramagnetic phase for almost all of the metastable region, with a slight increase in area of the ferromagnetic phase at smaller fields. This suggests that the mean-field approximation captures the phenomenology of both the metastable phases and their basins of attraction.

Note the contrast between the transition in $\overline{m}$ to the behavior of the magnetization m_{ss} of the steady state, cf. Fig. 5(a), which takes place for large Ω, outside the metastable parameter region. For the parameters where metastability is present, ρ_{ss} consists mostly of the ferromagnetic phase, $p_1^{\mathrm{ss}} \approx 1$. This shows that the short time evolution leads on average to the vast majority of initial states evolving to the paramagnetic metastable phase on short time scales, while at longer times they decaying into the mostly ferromagnetic stationary state.

The two metastable phases differ also in purity $\gamma = \mathrm{Tr}(\rho^2)$, see Figs. 5(e) and 5(f), with the ferromagnetic phase being almost pure ($\gamma_1 \approx 1$), in contrast the paramagnetic one almost completely mixed ($\gamma_2 \approx 1/2^N$). This is a consequence of the two phases corresponding respectively to inactive and active periods in the photon emission records [19]. The fluctuations in photon emissions per unit time for the system in the paramagnetic phase cause it to be a mixture of many different pure states, i.e., the large number of jumps causes these periods in the trajectories to consist of many different states, while the relative inactivity of the ferromagnetic phases leaves the state approximately pure. The relation of the metastable phases to activity in quantum trajectories is further studied in Sec. III E.

D. Expectations, correlations, and effective low-dimensional dynamics

After the initial relaxation the system state is approximately stationary during the metastable regime before eventual relaxation into the steady state. Metastability can be observed in the two-step decay of the expectation value $\langle O(t)\rangle$ and two-time correlation function $\langle O(t)O(0)\rangle$ of an observable O measured on the system. Here, we demonstrate that this is indeed the case when the observable is the magnetization M_z, Eq. (13).

We consider dynamics of two initial states: the "all up" state $\rho_\uparrow = (|\uparrow\rangle\langle\uparrow|)^{\otimes N}$, where $\sigma_z|\uparrow\rangle = |\uparrow\rangle$, and the "all right" state $\rho_\rightarrow = (|\rightarrow\rangle\langle\rightarrow|)^{\otimes N}$, where $\sigma_x|\rightarrow\rangle = |\rightarrow\rangle$. The expected values of the z magnetization, $\langle M_z(t)\rangle$, show a plateau in the metastable regime ($\tau' < t < \tau$), see Figs. 6(a) and 6(b), when the initial states evolve into mixtures of metastable phases, Fig. 6(e). Subsequent evolution takes the magnetization to that of the mostly ferromagnetic stationary state at later times ($t > \tau$). Meanwhile, the expected value of the x magnetization, $\langle M_x\rangle$, Figs. 6(c) and 6(d), displays oscillations for times $t < \tau'$ suggestive of those present in mean-field model, cf. Figs. 3(a)–3(c), which is expected to qualitatively represent the short-time dynamics. The long-time behavior is captured by the effective dynamics $\mathcal{L}_{\mathrm{eff}}$, cf. Eq. (8). Both states evolve mostly into a paramagnetic metastable phase $\langle M\rangle \approx 0$, despite differing considerably initially, $\mathrm{Tr}(\rho_\uparrow\rho_\rightarrow) = 1/2^N$. This demonstrates the dominance of this metastable phase in the short-time evolution.

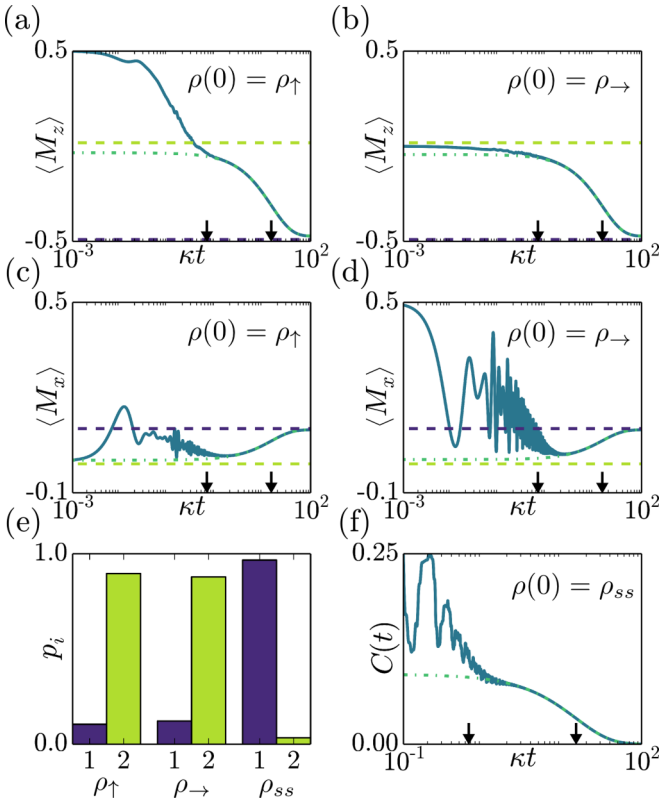

FIG. 6. Results calculated for parameters of $V/\kappa = 250$ and $\Omega/\kappa = 50$. (a) Time evolution of the average z magnetization, $\langle M_z\rangle$, for the initial state $\rho_\uparrow$. The z magnetizations of the metastable phases $\tilde{\rho}_{1,2}$ are represented by the dashed lines. (b) Same but for the initial state $\rho_\rightarrow$. [(c) and (d)] Time evolution of the average x magnetization, $\langle M_x\rangle$, for $\rho_\uparrow$ and $\rho_\rightarrow$. The average metastable values are given by dashed lines. (e) Histogram of the probability of finding $\rho_\uparrow$, $\rho_\rightarrow$, and ρ_{ss} in each eMS during the metastable regime, see Eq. (5) and (6). (f) Time-averaged autocorrelation function $C(t)$ of the projective measurement related to M_z in ρ_{ss} (see the main text). In panels (a)–(d) and (f) the time is in log scale, with the two arrows indicating the time scales τ' and τ. The exact dynamics is plotted as solid curves, and the effective dynamics as dash-dotted lines.

In Fig. 6(f) we show how metastability is also observed in the autocorrelation $C(t)$ of a measurement conducted on the steady state ρ_{ss}, see Eq. (9). We consider the observable $O = O_1 - O_2$, where O_1 is the sum of projections onto the $M_z = \pm 1/2N$ eigenspaces and $O_2 = |M_z = -1/2\rangle\langle M_z = -1/2|$, so the average of this observable gives the difference of probabilities of $P(M_z = \pm 1/2N)$ and $P(M = -1/2)$. Nonzero values of the magnetization are used as N is odd. We choose the correlations of O, which can be obtained from correlations of M_z by postselection, as they more clearly demonstrate the metastability. The initial measurement of O perturbs the stationary state from the metastable manifold. The relaxation towards the MM features large oscillations

in the autocorrelation $C(t)$, while relaxation at later times is described by $\mathcal{L}_{\text{eff}}$ and $C(t)$ is given by Eq. (10).

E. Intermittent dynamics of quantum trajectories

So far we have discussed the dynamics of the system described by the density matrix $\rho(t)$, which is governed by the master operator (1), and the related dynamics of observables on the system, such as the spin magnetization (13). Instead, one can consider an unravelling of a master equation into quantum trajectories [28], which corresponds to a particular experimental realization of system dynamics and a continuous measurement. In this case, a quantum jump occurs when, say, the system jump operator J_k flips the kth spin from up to down, cf. Eq. (12), which is accompanied by the emission of a photon into the environment, which can be detected. In this case, a measurement record up to time t consists of information about which spins emitted photons and the emission times, see Figs. 7(b) and 7(c).

Based on this record, a quantum trajectory—the conditional pure system state at any time $t' \leqslant t$—can be reconstructed [28]. The density matrix $\rho(t)$ considered in earlier sections is simply an average over the ensemble of such pure conditional states at time t, i.e., over the system state at time t in all realizations of the experiment. We now discuss how metastability is present not only in the master equation dynamics but also in individual quantum trajectories.

Photon emission records and quantum trajectories can be generated by the quantum jump Monte Carlo method (see, e.g., Ref. [7]). The probability of observing no photon emission for time t' for the system initially in $|\psi\rangle$ is given by $P_0(t') = \langle\psi(t')|\psi(t')\rangle$, where $|\psi(t')\rangle = e^{it'H_{\text{eff}}}|\psi\rangle$ with the effective Hamiltonian $H_{\text{eff}} = H - \frac{i}{2}\sum_{j=1}^{N} J_j^\dagger J_j$, cf. (11) and (12). The probability of observing a first photon emission from a jth spin at time t' is further given by $P_j(t') = \langle\psi(t')| J_j^\dagger J_j |\psi(t')\rangle$, and the conditional pure system state is $|\psi_j(t')\rangle = J_j|\psi(t')\rangle / \sqrt{P_j(t')}$. Using these definitions one can simulate the system evolution in terms of stochastic quantum trajectories [7].

The total number of photons emitted up to time t for dynamics with a unique steady state obeys the central limit theorem [43,44]. Moreover, both the mean and the variance of the total number of emissions asymptotically ($t \gg \tau$) scale linearly with time t (for the case of the dissipative Ising model see Ref. [19]). We argue that this also holds in the metastable regime for each of the metastable phases. As the total emission number $\Lambda(t)$ is an observable integrated over the observation time, for time t well inside the metastability regime, the leading terms in its mean and variance are given by the contribution when the system state (averaged over trajectories) is metastable. Since the instantaneous rate μ of photon emissions from the system in a state ρ is given by its magnetization, $\mu = \sum_{j=1}^{N} \text{Tr}(J_j^\dagger J_j \rho) = N\kappa[\text{Tr}(M_z\rho) + \frac{1}{2}]$, the mean number of photons emitted in time $\tau' \ll t \ll \tau$ can be approximated by $\langle\Lambda(t)\rangle \approx t\, N\, \kappa\, (p_1 m_1 + p_2 m_2 + \frac{1}{2})$.

Consider the case of an initial state evolving into just one of the metastable phases. In that case the mean activity, $k(t) = \Lambda(t)/t$, of trajectories is given by the magnetization in the corresponding eMS, $\langle k(t)\rangle \approx N\kappa(m_1 + \frac{1}{2})$ or $N\kappa(m_2 + \frac{1}{2})$. As the correlations of dynamics inside a metastable phase can decay at most at times of order τ', in this case also the variance, $\Delta^2\Lambda(t)$, scales linearly in time for t within the metastable regime. This means that the variance of the activity, $\Delta^2 k(t)$, is inversely proportional to t. If the metastable regime is long enough, the fluctuations of activity around its mean value, $N\kappa(m_{1,2} + \frac{1}{2})$, are small and trajectories can be classified as "active" (large k) or "inactive" (small k). Note that when an initial state evolves at the beginning of the metastable regime into a mixture of two eMSs, $p_1\tilde{\rho}_1 + p_2\tilde{\rho}_2$, the activity statistics is determined mostly by the contribution from the metastable regime, and thus emission records are a mixture of the active and inactive records.

Now consider a *coarse graining* in time of the photon emission records, where an emission record is divided into time bins of size t_{bin} and the emission record is replaced by the activity of time bins. It is known that for intermittent dynamics the time-bin activity distribution can be bimodal [19]. From the arguments above it follows that for a t_{bin} well inside the metastable regime that is long enough, the

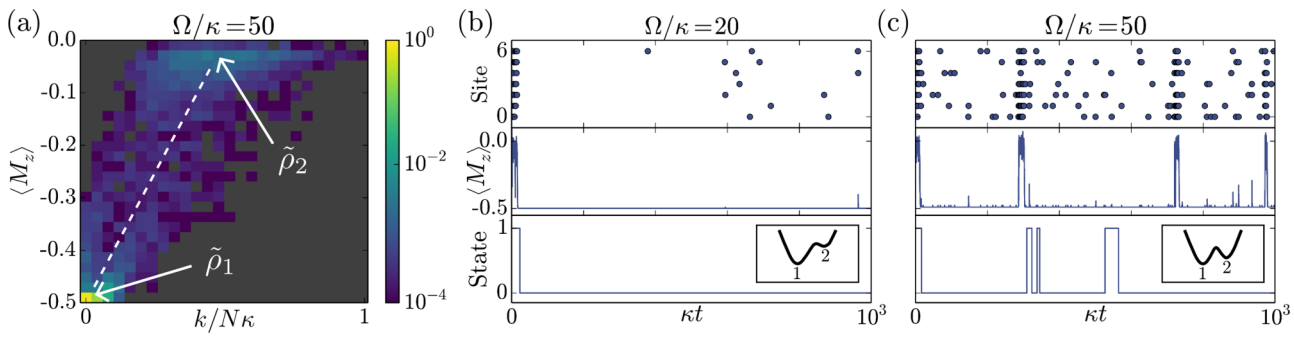

FIG. 7. (a) A 2D histogram of the average magnetization m and activity k of time bins of length $t_{\text{bin}} = 6\tau'$, for parameters $V/\kappa = 250$, $\Omega/\kappa = 50$, and $N = 7$. The arrows indicate the expectation values for $\tilde{\rho}_1$ and $\tilde{\rho}_2$, respectively, with the decay $e^{t_{\text{bin}}\lambda_2}$ of R_2 taken into account. The white dashed line indicates the relation $\langle k\rangle/N\kappa = \langle M_z\rangle + \frac{1}{2}$. [(b) and (c)] Sample trajectories for two different sets of parameters in the metastable region, $V/\kappa = 250$ with $\Omega/\kappa = 20$, 50, for $N = 7$ and time in linear scale. The first and seconds rows show the space- and time-resolved photon emissions and the corresponding magnetization of the state over time, respectively, for a sample QJMC trajectory. The third row shows a sample classical trajectory, jumping between the two metastable phases. The insets on the third row show sketches of the double-well potentials of free energy leading to analogous classical evolution between the metastable states of two wells.

probability distribution of activity is indeed bimodal with inactive dynamics corresponding to magnetization of the ferromagnetic phase $m_1 \approx -0.5$ and the active dynamics corresponding to the paramagnetic phase $m_2 \approx 0$, which is visible in Fig. 7(a). This demonstrates that the periods of active and inactive dynamics (so-called dynamical phases [11]) correspond to directly to two metastable phases.

We now discuss the relation between intermittency and the effective dynamics. For times after initial relaxation $t \gg \tau'$ the system dynamics $\rho(t)$ can be obtained as an average over classical trajectories generated by $\mathcal{L}_{\text{eff}}$, Eq. (7), between two metastable phases. Those classical trajectories are ergodic, i.e., a time-averaged state in a trajectory approaches the steady state ρ_{ss} for $t \to \infty$, which requires the ratio of time spent in each of the metastable phases to be given by $p_1^{\text{ss}}/p_2^{\text{ss}} = -c_2^{\min}/c_2^{\max}$, cf. Eq. (7). On the other hand, we know that the emission record coarse grained in time consists of active and inactive periods with small fluctuations. As the activity of a long record approaches the emission rate of the steady state, $\langle k \rangle_{\text{ss}} = \mu_{\text{ss}} = N\kappa(m_{\text{ss}} + \frac{1}{2})$, the probabilities of the inactive and active dynamics are again given (approximately) by p_1^{ss} and p_2^{ss} [see Fig. 7(a)]. Finally, the average length of active or inactive dynamics in coarse-grained records cannot exceed the longest time scale τ of the model. This yields a direct relation between the classical trajectories and the coarse-grained intermittent emission records, see Figs. 7(b) and 7(c).

The classical dynamics generated by $\mathcal{L}_{\text{eff}}$ can be related back to the double-well model discussed in Sec. II, with the sketches of the relevant double-well potential shown in the insets of Fig. 7(b) and 7(c). The smaller spectral gap $-\lambda_2$ for Fig. 7(c) leads to longer periods spent in two phases, analogous to a higher barrier between the wells, and results in a longer equilibration time. When the difference in probabilities between the metastable phases in ρ_{ss}, $|p_1^{\text{ss}} - p_2^{\text{ss}}| = |c_2^{\max} + c_2^{\min}|/\Delta c_2$, is larger [Fig. 7(b)], the times spent in the two states differ more, analogously to how the bigger differences in the free energies of the two wells makes time spent in the well of higher free energy shorter and hence less of the equilibrium state is supported there.

The average over the ensemble of quantum trajectories also gives the dynamics of the system state $\rho(t)$. It is not generally known if those trajectories are ergodic, i.e., whether each time-averaged trajectory asymptotically gives the steady state. If that was the case, as the supports of metastable phases are approximately disjoint [25], then one could expect the quantum trajectories to be ergodic also inside those supports for $\tau' \ll t \ll \tau$, which would lead to the classical trajectories being the coarse graining of quantum ones. By considering the magnetization of a quantum trajectory, due to its relation to the photon emission activity, one indeed recovers the effective dynamics up to fluctuations within the τ' time scale, see Figs. 7(b) and 7(c).

IV. CONCLUSIONS

We have applied the general theory of metastability developed recently in Ref. [25] to the dynamics of an open many-body quantum system, namely the open quantum Ising model with transverse field in the presence of site decay, a model which could potentially be realized using Rydberg atoms. For this system the origin and properties of the metastable dynamics is particularly transparent: In a region of parameter space where interactions and the transverse field compete there is time separation in the dynamics such that the two leading eigenmodes of the master operator split from the rest. This means that the metastable manifold to which an initial state decays at short times is a one-dimensional simplex given by the convex combinations of two extreme metastable states. These two states represent the two metastable phases of the problem, an almost pure state of negative magnetization in the z direction and one mixed state of almost vanishing magnetization. We have also shown that the dynamics of this model at long times can be understood in terms of an effective classical dynamics between two phases inside the metastable manifold, which converges to the unique stationary state asymptotically.

We have also shown that the short-time behavior and the existence of the long-lived metastable states are qualitatively captured by a straightforward mean-field approximation to the dynamics, very much in the spirit of what one does in slowly relaxing classical systems. We have also discussed how metastability is directly related to fluctuating dynamics in individual realizations of the system evolution, specifically in the form of intermittency of quantum jump trajectories. The physical ingredients that give rise to metastability in the model studied here are those that could also be responsible for the system having a true stationary state phase transition in the thermodynamic limit. But just like in the case of analogous classical problems, the dynamics we uncovered (separation of time scales, transient relaxation to long-lived states, intermittency due to switching between metastable phases) is not dependent on that transition being present, as metastability would occur in systems where the transition is avoided either through finite size or due to other kind of fluctuations.

The concrete application of the ideas of Ref. [25] to a many-body system should pave the way for further studies of metastability in other systems with even richer emergent collective dynamics, in particular systems where the manifold of long-lived states is higher dimensional, potentially allowing for quantum mechanical evolution between these states.

ACKNOWLEDGMENTS

The research leading to these results has received funding from the European Research Council under the European Union's Seventh Framework Programme (FP/2007-2013)/ERC Grant Agreement No. 335266 (ESCQUMA). We also acknowledge financial support from EPSRC Grant No. EP/M014266/1 and from the H2020-FETPROACT-2014 Grant No. 640378 (RYSQ). We are also grateful for access to the University of Nottingham High Performance Computing Facility. We thank A. A. Gangat for bringing Ref. [18] to our attention.

[1] J. D. Pritchard, D. Maxwell, A. Gauguet, K. J. Weatherill, M. P. A. Jones, and C. S. Adams, Cooperative Atom-Light Interaction in a Blockaded Rydberg Ensemble, Phys. Rev. Lett. **105**, 193603 (2010).

[2] R. Blatt and C. F. Roos, Quantum simulations with trapped ions, Nat. Phys. **8**, 277 (2012).

[3] J. W. Britton, B. C. Sawyer, A. C. Keith, C. C. J. Wang, J. K. Freericks, H. Uys, M. J. Biercuk, and J. J. Bollinger, Engineered two-dimensional Ising interactions in a trapped-ion quantum simulator with hundreds of spins, Nature **484**, 489 (2012).

[4] Y. O. Dudin and A. Kuzmich, Strongly interacting Rydberg excitations of a cold atomic gas, Science **336**, 887 (2012).

[5] T. Peyronel, O. Firstenberg, Q. Liang, S. Hofferberth, A. V. Gorshkov, T. Pohl, M. D. Lukin, and V. Vuletic, Quantum nonlinear optics with single photons enabled by strongly interacting atoms, Nature **488**, 57 (2012).

[6] G. Günter, H. Schempp, M. Robert-de Saint-Vincent, V. Gavryusev, S. Helmrich, C. S. Hofmann, S. Whitlock, and M. Weidemüller, Observing the dynamics of dipole-mediated energy transport by interaction-enhanced imaging, Science **342**, 954 (2013).

[7] A. J. Daley, Quantum trajectories and open many-body quantum systems, Adv. Phys. **63**, 77 (2014).

[8] L. M. Sieberer, M. Buchhold, and S. Diehl, Keldysh field theory for driven open quantum systems, Rep. Prog. Phys. **79**, 096001 (2016).

[9] M. F. Maghrebi and A. V. Gorshkov, Nonequilibrium many-body steady states via Keldysh formalism, Phys. Rev. B **93**, 014307 (2016).

[10] Emanuele G. Dalla Torre, S. Diehl, M. D. Lukin, S. Sachdev, and P. Strack, Keldysh approach for nonequilibrium phase transitions in quantum optics: Beyond the Dicke model in optical cavities, Phys. Rev. A **87**, 023831 (2013).

[11] J. P. Garrahan and I. Lesanovsky, Thermodynamics of quantum jump trajectories, Phys. Rev. Lett. **104**, 160601 (2010).

[12] I. Lesanovsky, M. van Horssen, M. Guţă, and J. P. Garrahan, Characterization of dynamical phase transitions in quantum jump trajectories beyond the properties of the stationary state, Phys. Rev. Lett. **110**, 150401 (2013).

[13] M. Esposito, U. Harbola, and S. Mukamel, Nonequilibrium fluctuations, fluctuation theorems, and counting statistics in quantum systems, Rev. Mod. Phys. **81**, 1665 (2009).

[14] P. M. Chaikin and T. C. Lubensky, *Principles of Condensed Matter Physics* (Cambridge University Press, Cambridge, 2000), Vol. 1.

[15] K. Binder and W. Kob, *Glassy Materials and Disordered Solids: An Introduction to Their Statistical Mechanics (Revised Edition)* (World Scientific, Singapore, 2011).

[16] G. Biroli and J. P. Garrahan, Perspective: The glass transition, J. Chem. Phys. **138**, 12A301 (2013).

[17] T. E. Lee, H. Häffner, and M. C. Cross, Collective Quantum Jumps of Rydberg Atoms, Phys. Rev. Lett. **108**, 023602 (2012).

[18] O. Viehmann, J. von Delft, and F. Marquardt, Observing the Nonequilibrium Dynamics of the Quantum Transverse-Field Ising Chain in Circuit QED, Phys. Rev. Lett. **110**, 030601 (2013).

[19] C. Ates, B. Olmos, J. P. Garrahan, and I. Lesanovsky, Dynamical phases and intermittency of the dissipative quantum Ising model, Phys. Rev. A **85**, 043620 (2012).

[20] H. Weimer, Variational principle for steady states of dissipative quantum many-body systems, Phys. Rev. Lett. **114**, 040402 (2015).

[21] H. Weimer, Variational analysis of driven-dissipative Rydberg gases, Phys. Rev. A **91**, 063401 (2015).

[22] V. R. Overbeck, M. F. Maghrebi, A. V. Gorshkov, and H. Weimer, Multicritical behavior in dissipative Ising models, arXiv:1606.08863 (2016).

[23] M. Marcuzzi, M. Buchhold, S. Diehl, and I. Lesanovsky, Absorbing state phase transition with competing quantum and classical fluctuations, Phys. Rev. Lett. **116**, 245701 (2016).

[24] A. A. Gangat, Te I, and Y.-J. Kao, Steady states of infinite-size dissipative quantum chains via imaginary time evolution, arXiv:1608.06028 (2016).

[25] K. Macieszczak, M. Guta, I. Lesanovsky, and J. P. Garrahan, Towards a Theory of Metastability in Open Quantum Dynamics, Phys. Rev. Lett. **116**, 240404 (2016).

[26] G. Lindblad, On the generators of quantum dynamical semigroups, Commun. Math. Phys. **48**, 119 (1976).

[27] V. Gorini, A. Kossakowski, and E. C. G. Sudarshan, J. Math. Phys. **17**, 821 (1976).

[28] H. P. Breuer and F. Petruccione, *The Theory of Open Quantum Systems* (Oxford University Press, Oxford, 2002).

[29] B. Gaveau and L. S. Schulman, Dynamical metastability, J. Phys. A **20**, 2865 (1987).

[30] B. Gaveau and L. S. Schulman, Theory of nonequilibrium first-order phase transitions for stochastic dynamics, J. Mat. Phys. **39**, 1517 (1998).

[31] A. Bovier, M. Eckhoff, V. Gayrard, and M. Klein, Metastability and low lying spectra in reversible Markov chains, Comm. Math. Phys **228**, 219 (2002).

[32] B. Gaveau and L. S. Schulman, Multiple phases in stochastic dynamics: Geometry and probabilities, Phys. Rev. E **73**, 036124 (2006).

[33] J. Kurchan, Six out of equilibrium lectures, arXiv:0901.1271 (2016).

[34] J. Thingna, D. Manzano, and J. Cao, Dynamical signatures of molecular symmetries in nonequilibrium quantum transport, Sci. Rep. **6**, 28027 (2016).

[35] It is possible that the master operator may not be completely diagonalizable, in which in this case its simplest form is the Jordan normal form. Under exponentiation this gives rise to a polynomial dependence on the time; however, this is accompanied by the usual exponential evolution. The part of the spectrum we are concerned with is assumed to be diagonalizable (as is the case for this model) and any polynomial evolution is thus dominated by the decaying exponentials on the relevant time scales.

[36] L. S. Schulman and B. Gaveau, Coarse grains: The emergence of space and order, Found. Phys. **31**, 713 (2001).

[37] B. Sciolla, D. Poletti, and C. Kollath, Two-Time Correlations Probing the Dynamics of Dissipative Many-Body Quantum Systems: Aging and Fast Relaxation, Phys. Rev. Lett. **114**, 170401 (2015).

[38] M. Müller, L. Liang, I. Lesanovsky, and P. Zoller, Trapped Rydberg ions: From spin chains to fast quantum gates, New J. Phys. **10**, 093009 (2008).

[39] S. G. Schirmer and X. Wang, Stabilizing open quantum systems by Markovian reservoir engineering, Phys. Rev. A **81**, 062306 (2010).

[40] M. Marcuzzi, E. Levi, S. Diehl, J. P. Garrahan, and I. Lesanovsky, Universal Nonequilibrium Properties of Dissipative Rydberg Gases, Phys. Rev. Lett. **113**, 210401 (2014).

[41] B. Buča and T. Prosen, A note on symmetry reductions of the Lindblad equation: transport in constrained open spin chains, New J. Phys. **14**, 073007 (2012).

[42] V. V. Albert and L. Jiang, Symmetries and conserved quantities in Lindblad master equations, Phys. Rev. A **89**, 022118 (2014).

[43] M. Guta, Fisher information and asymptotic normality in system identification for quantum Markov chains, Phys. Rev. A **83**, 062324 (2011).

[44] C. Catana, L. Bouten, and M. Guta, Fisher informations and local asymptotic normality for continuous-time quantum Markov processes, J. Phys. A **48**, 365301 (2015).